Connectivity of the bay scallop (*Argopecten irradians*) in Buzzards Bay, Massachusetts, USA

Chang Liu[1], Geoffrey W. Cowles[1,*], James H. Churchill[2], and Kevin D.E. Stokesbury[1]

[1]*Department of Fisheries Oceanography*

School for Marine Sciences and Technology

University of Massachusetts Dartmouth

706 S Rodney French Blvd, New Bedford, MA 02744, USA

[2]*Department of Physical Oceanography*

Woods Hole Oceanographic Institution

Woods Hole, MA 02543, USA

*Corresponding author:

gcowles@umassd.edu

Running title: Connectivity of the bay scallop in Buzzards Bay

ABSTRACT

The harvest of bay scallops (*Argopecten irradians*) from Buzzards Bay, Massachusetts, USA undergoes large interannual fluctuations, varying by more than an order of magnitude in successive years. To investigate the extent to which these fluctuations may be due to yearly variations in the transport of scallop larvae from spawning areas to suitable juvenile habitat (settlement zones), a high-resolution hydrodynamic model was used to drive an individual-based model of scallop larval transport. Model results revealed that scallop spawning in Buzzards Bay occurs during a time when nearshore bay currents were principally directed up-bay in response to a persistent southwesterly sea breeze. This nearshore flow results in substantial transport of larvae from lower-bay spawning areas to settlement zones further up-bay. Averaged over the entire bay, the spawning-to-settlement zone connectivity exhibits little interannual variation. However, connectivities between individual spawning and settlement zones vary by up to an order of magnitude. The model results identified spawning areas that have the greatest probability of transporting larvae to juvenile habitat. Because managers may aim to increase scallop populations either locally or broadly, the high-connectivity spawning areas were divided into: 1) high larval retention and relatively little larval transport to adjoining settlement areas, 2) both significant larval retention and transport to more distant settlement areas, and 3) little larval retention but significant transport to distant settlement areas.

Key words: Individual-based model, connectivity, bay scallop, *Argopecten irradians*, Lagrangian tracking, Buzzards Bay

INTRODUCTION

The bay scallop (*Argopecten irradians*) has been the foundation of a historically important fishery in Buzzards Bay, Massachusetts, USA (Belding, 1910, 1931; MacFarlane, 1999). As indicated by landing data compiled by the Massachusetts Division of Marine Fisheries (MassDMF), the annual harvest of bay scallops from Buzzards Bay has varied significantly in the last six decades (Fig. 1). This variation is marked by large year-to-year changes (i.e., a drop from 215,040 kg in 1985 to 10,312 kg in 1986) and longer trends (annual harvests of > 150,000 kg over 1968-1972 vs. harvest of < 3,000 kg over 1988-1991). The underlying causes of such variations are clearly of interest to managers tasked with minimizing the number of years with low scallop harvest (MacFarlane, 1999).

Along the eastern seaboard of the United States there are several subspecies of bay scallops, with the northernmost subspecies, *A. irradians irradians*, residing in Massachusetts waters. The life cycle of *A. irradians irradians* is typically two years (Blake and Shumway, 2006), a notable distinction from the southern subspecies which is comprised of a single year class. Bay scallop populations are comprised of one or two year classes due to this life span and abundance and harvests are highly sensitive to variations in the annual recruitment success. Among the factors that may contribute to the variation in recruitment success to the early juvenile stage are predation (McNamara *et al.*, 2010), spawning density (Tettelbach *et al.*, 2013), juvenile size (Bishop *et al.*, 2005; Tettelbach *et al.*, 2001), eelgrass abundance (Belding, 1910), and the degree to which pelagic bay scallop larvae are carried by marine currents from spawning sites to suitable juvenile habitat (Le Pennec *et al*., 2003).

The last factor is routinely studied with an Individual-Based Modeling (IBM) approach, which involves driving a Lagrangian larval transport model with fields of currents and ocean properties generated by an ocean circulation model. IBMs have been employed to examine various aspects of spawning-to-nursery-area connectivity, including: connectivity between specific regions (e.g., Siegel *et al.*, 2008; Xue *et al.*, 2008), larval retention within a given region (e.g., Banas *et al.*, 2009; Churchill *et al.*, 2011), and the effects of physical forcing on larval dispersal (e.g., Tian *et al.*, 2009a).

The timing of the bay scallop spawning exhibits a latitudinal gradient with higher latitudes spawning later in the season. In Massachusetts waters, most spawning occurs during June and July (Belding, 1910; Taylor and Capuzzo, 1983; Bricelj *et al.*, 1987). Spawned eggs take on a spherical form and are commonly located near the bottom of the water column. The total time from egg fertilization to the settlement-capable phase, or the pelagic larval duration (PLD), is typically no longer than 14 days (Belding, 1910; Loosanoff and Davis, 1963; Sastry, 1965; MacKenzie, 2008),. During this period scallop larvae are subject to transport by marine currents. As adult bay scallops tend to remain stationary (Belding, 1910), the larval stage is the most critical in terms of individual movement and population dispersal.

Buzzards Bay, is a shallow embayment with a mean depth of 11 m and approximate dimensions of 45 km in the lengthwise (SW-NE) direction and 12 km in the transverse direction (NW-SE) (Fig. 2, Lower Panel). Along its southeastern edge Buzzards Bay is connected to Vineyard Sound via several narrow openings (e.g., Quicks Hole and Woods Hole). The density-driven flow in the bay is weak (order 1 cm/s) relative to the wind and tidally-driven flow (Signell, 1987). The tidal response in the bay is effectively a standing wave, with tidal currents of <5 cm s^{-1} over most of the bay. The tidal signal is complicated

in regions near the passageways separating the bay from Vineyard Sound, as well as near the Cape Cod Canal, where differences in the tidal amplitude and phase between the adjacent bodies of water drive strong currents and contribute to a complex residual flow field (Signell, 1987).

The wind forcing over Buzzards Bay is seasonal, with NW (cross-bay) winds dominant over the late fall to early spring and the SW (along-bay) sea breeze dominant between June and September (Signell, 1987). A key aspect of the summertime circulation is a two-way flow driven by the along-bay wind forcing. When this circulation is in place, the depth-averaged flow is downwind in the shallow regions along the bay's edges and is upwind in the deeper interior of the bay (Csanady, 1973; Signell, 1987).

There is no targeted survey for bay scallops in Buzzards Bay. The MassDMF conducts an inshore dredge survey in the fall and spring, but the survey vessel's draft limitation excludes much of the bay's known scallop habitat. As the majority of scallops spawn only once during their short life span and fisherman are allowed to harvest the entire second year class following the spawning season, catch serves as a proxy for the bay scallop abundance (MacKenzie, 2008).

Here we used an IBM approach to investigate bay scallop larval dispersal and spawning-to-settlement-zone connectivity in Buzzards Bay. The primary motivation was to explore the extent to which yearly variations in connectivity may be responsible for the large yearly variations in bay scallop harvest, but other questions relevant to managing bay scallop stocks in Buzzards Bay were also considered. These include: *1*) Which known bay scallop spawning areas have the highest larval connectivity with settlement zones and may thus be candidates for enhanced protection?; 2) What are the important geographical pathways of scallop larval transport from spawning areas to settlement zones within

Buzzards Bay?; and 3) What physical processes are most important in controlling spawning-to-settlement zone connectivity in Buzzards Bay?

METHODS

Physical model

The Finite-Volume Community Ocean Model (FVCOM) was employed to compute the hydrodynamic fields (Chen *et al.*, 2003, 2006; Cowles, 2008) used for larval scallop tracking. An open source model with over 2500 registered users, FVCOM has been successfully applied to a wide array of coastal and open ocean studies (Chen *et al.*, 2008, 2011; Cowles *et al.*, 2008). The kernel of FVCOM computes a solution of the hydrostatic primitive equations on an unstructured grid in the horizontal plane using a second-order accurate finite-volume formulation for spatial fluxes (Kobayashi *et al.*, 1999). The vertical coordinate is discretized using a generalized terrain-following approach.

Modeling of Buzzards Bay was done using the high-resolution Southeastern Massachusetts (SEMASS) FVCOM model (Fig. 2). The vertical model domain was discretized using 30 evenly spaced σ-layers. The total number of grid cells (control volumes) was 255,033. Horizontal model-grid resolution varied from 5 km over the outer shelf to 500 m along the coast. The resolution was further enhanced within Cape Cod Canal (100 m) and Buzzards Bay (50 m).

The SEMASS model was embedded, through one-way nesting, in a larger, regional-scale Gulf of Maine (GoM) FVCOM model (Fig. 2, upper panel), which provided open boundary forcing for the SEMASS model. Based on an early generation of the Northeast Coastal Ocean Forecast System (NeCOFS, 2013), the GoM model consisted of 27,571

control volumes and was forced with hydrography and sea surface height at the open boundary, buoyancy flux from the major regional rivers, and wind stress and heat flux derived from regional hindcasts of the Weather Research and Forecasting (WRF) model (see Cowles *et al.*, 2008 for details).

Individual-based model

Larval tracking used an open-source IBM package, the FVCOM I-State Configuration Model (FISCM; FISCM, 2013). FISCM has been employed in studies on the transport and retention of haddock larvae on Georges Bank (Petrik, 2011; Boucher *et al.*, 2013), and the physiological factors controlling the biogeographical boundaries of several Arctic and sub-Arctic copepods species (Ji *et al.*, 2011).

FISCM determined the advection of each individual through

$$\frac{d}{dt}\vec{X}(t) = \vec{V}(\vec{X}(t), t), \tag{1}$$

where $\vec{X}(t)$ is the three-dimensional position of the individual at time t and $\vec{V}(\vec{X}(t),t)$ is the velocity field. $\vec{V}(\vec{X}(t),t)$ was computed by bi-linearly interpolating the flow field output from FVCOM. Updating particle position from $\vec{X}(t)$ to $\vec{X}(t+\Delta t)$ was accomplished by integrating $\vec{V}(\vec{X}(t),t)$ with 4th-order explicit 4-stage Runge-Kutta scheme (ERK4) and a fixed time step, Δt, of 240 s. A vertical random walk formulation from Visser (1997) was implemented to statistically account for the effects of vertical diffusivity through:

$$\begin{aligned} z(t+\delta t) =& z(t) + \left.\frac{\partial K_v}{\partial z}\right|_{z(t)} \delta t \\ &+ R\sqrt{\frac{2}{r}K_v\left(z(t) + \frac{1}{2}\left.\frac{\partial K_v}{\partial z}\right|_{z(t)}\delta t\right)\delta t}, \end{aligned} \tag{2}$$

where, z is the vertical coordinate, positive down; R is a random factor producing a normal distribution with zero mean and variance $r = < R^2 >$; K_v is the vertical diffusivity provided by FVCOM output; and δt is the sub-time step for vertical random walk. The vertical random walk was implemented with a time step $\delta t = \Delta t / n$, where n=10.

Boundary conditions were implemented for "individuals" crossing the model boundaries to ensure that the number of individuals was conserved. If an individual moved across a horizontal land or open-ocean boundary during a time step, it was restored to its last position (from the previous time step) within the model domain. The extent of the SEMASS domain is large compared with Buzzards Bay (Fig. 2, upper panel) and thus the no-penetration condition at the open boundary does not influence the results of this work. If an individual moved above or below the water column due to advection or diffusion, it was reflected back into the water column according to:

$$z(t+\delta t) = \begin{cases} -z(t+\delta t), & : \text{if } z(t+\delta t) < 0 \\ 2H - z(t+\delta t), & : \text{if } z(t+\delta t) > H \end{cases}, \tag{3}$$

where z is the vertical coordinate (downward positive) and H is the depth of the water column in which the individual is located at time t.

Determination of Lagrangian probability density functions and connectivities

To quantify connectivity, we used the results from the IBM simulation to determine Lagrangian Probability Density Functions (LPDFs). LPDF approaches have been widely used in processing dispersal patterns driven by turbulent processes (Mitarai *et al.*, 2009; Roughan *et al.*, 2011).

Following Mitarai *et al.* (2009), an LPDF $f_\psi(\vec{x},\tau)$ was defined as the probability density (probability per unit area) of an individual from a group of individuals ψ being at a location $\vec{x}$=(*x*,*y*) at larval age τ . To construct the LPDF, we selected the 2-D kernel density estimator (Botev *et al.*, 2010). The kernel density estimator is a computationally efficient, non-parametric technique for estimation of probability density functions. Given a set of particle locations $\psi \equiv (\overrightarrow{X_1}(\tau), \overrightarrow{X_2}(\tau), \ldots, \overrightarrow{X_n}(\tau))$, the corresponding 2-D Gaussian kernel at the specific larval age τ

$$G(\vec{x}, \vec{X}_i(\tau), c) = \frac{1}{2\pi c^2} e^{-\left(\vec{x}-\vec{X}_i(\tau)\right)^2/(2c^2)} \tag{4}$$

was used to quantify the LPDF

$$f_\psi(\vec{x},\tau) = \frac{1}{N}\sum_{i=1}^{N} G(\vec{x}, \vec{X}_i(\tau), c), \tag{5}$$

where *c* is a spatial scale commonly referred to as the bandwidth, which is determined optimally by the Botev *et al.* (2010) method. Note that the dimension of the LPDF $f_\psi(\vec{x},\tau)$ is 1/(distance^2). The procedure of constructing LPDFs numerically was to: 1) bin the particle locations into an *n*-by-*n* square grid, 2) calculate the probability density in each grid cell by dividing the number of particles that fall in this cell by the size of the cell, and 3) smooth the probability density field using Gaussian kernels with the optimized bandwidth *c*. The optimal binning resolution parameter *n*, which is the number of boxes on one side of the square grid used for binning, was *n*=128 based on a sensitivity study.

In the model, larvae were considered capable of settling over 10-14 days of the PLD. Assuming a uniform probability of settlement over this age range, $f_\psi(\vec{x},\tau)$ was used to determine a settlement PDF, F_ψ according to

$$F_{\psi}(\vec{x}) = \frac{1}{4}\int_{10}^{14} f_{\psi}(\vec{x},\tau)d\tau. \quad (6)$$

$F_{\psi}(\vec{x})$ can be interpreted as the probability density that a larva from group ψ will settle at a location $\vec{x}$, assuming mortality over the larval duration is zero.

The connectivity between a spawning region *i* and a settlement zone *j*, denoted as P_{ij}, was defined as the probability that larvae spawned in *i* during some specified time period successfully settle in *j*. It was determined by integrating F_{ψ} over the area of *j* and by specifying that the ψ represent those larvae spawned in zone *i, i.e.:*

$$P_{ij} = \iint_{A_j} F_j(\vec{x})\mathrm{dA}, \quad (7)$$

where A_j is the area of settlement zone *j*.

Defining spawning and settlement zones

Regions defining the areas of spawning and settlement were delineated but did not always coincide because the distribution of adult bay scallops and the habitats to which larvae are able to successfully recruit are often not identical (S. Tettelbach, Long Island University, USA, pers. comm.). Spawning zones were established using bay scallop suitability areas identified by MassDMF based on observations of the adult distribution (MA DFG, 2009). These suitability areas were then divided into discrete zones using state-designated shellfish growing areas (Fig. 3a). Spawning zones encompassed 119 km^2, 18.5% of the total area of Buzzards Bay. Settlement zones were defined based on the habitat where larvae are able to successfully settle, which includes beds of eelgrass *Zostera marina L.* and other submerged aquatic vegetation (Thayer and Stuart, 1974; Carroll *et al.*, 2010). We were not able to comprehensively map the eelgrass distribution in Buzzards Bay as recent eelgrass surveys

of the bay were conducted only in select embayments (Costello and Kenworthy, 2011). However, based on the observed coverage of eelgrass (BBNEP, 2012), we determined that eelgrass is generally found in areas with depth not exceeding 3.5 m. Areas meeting this depth constraint were used as an estimate of the extent of submerged aquatic vegetation beds for our model study. These areas (14.7% of Buzzards Bay) were divided into distinct settlement zones that coincided approximately with the spawning zones (Fig. 3b). Two additional settlement zones, with no corresponding spawning zones, were defined along the Elizabeth Islands. To examine the broad pattern of larval transmission, the spawning and settlement zones were grouped into five regions: Zones 1–7 (Lower-Bay, LB), Zones 8–14 (Mid-Bay, MB), Zones 15–23 (Upper-Bay, UB), Zones 24–25 (East-Bay, EB), and Zones 26–27 (Elizabeth Islands, EI; settlement only).

Model experiments

Both realistic and idealized test cases (Table 1) were used to address the questions posed in the Introduction. For the realistic cases, the coupled biophysical model was used to simulate both early (25 June – 6 July) and later (25 July – 6 August) spawning for 2008–2010, allowing us to examine the influence of both seasonal and interannual hydrodynamic forcing variability on the transport of larvae.

Physical fields for the IBM were generated by realistic hydrodynamic hindcasts over 1 June – 1 September for 2008–2010. At the surface, the SEMASS model was forced with uniform horizontal wind forcing, derived from the wind record of the Buzzards Bay Buoy (BUZM3), obtained from the National Data Buoy Center. Output from the SEMASS hindcast was archived at hourly intervals and used to drive FISCM. For all cases, winds

recorded at BUZM3 were SW-dominant, with the prevailing and mean wind direction falling in the third quadrant (between 180°and 270°; Table 2).

For the idealized cases, the SEMASS was forced by either tides only or a combination of tides and an idealized wind field. In Case I1, SEMASS was set up using a constant density ocean and forced only by M_2 tides. The setup was the same for Case I2, but with additional forcing of a spatially and temporally constant 10 m s^{-1} SW wind. In Case I3, SEMASS was forced by the M_2 tide in combination with an idealized time-dependent wind representing the sea breeze in Buzzards Bay. To construct the idealized wind signal, daily-averaged wind data from BUZM3 were used to determine the variance, peak magnitude, and time of peak magnitude of the SW sea breeze. These characteristics were used to establish the idealized wind as a diurnal SW wind with a time-dependent magnitude described by the Gaussian function:

$$V(t) = \sum_n V_{max} \cdot e^{-\frac{(t-t_p)^2}{2\cdot\sigma^2}}, t_p = 16 + 24n, n = 0, 1, ... \quad (8)$$

where t is time in h after midnight of the initial simulation day, and the standard deviation, σ, is 3 h. The peak magnitude V_{max}= 12 m s^{-1} occurs daily at 16:00 (t_p=16 h) U.S. Eastern daylight time. For Case I4, SEMASS was driven by BUZM3 winds over the period 20 December 2009 to 19 January 2010. These winds were NW dominant (prevailing direction: 310°, mean direction: 320.3°, angular standard deviation: 47.4°), characteristic of the winter season. The purpose of this idealized case was to evaluate the connectivity due to wind forcing different from that of the summer spawning period.

A total of 47,631 neutrally buoyant "individuals" were released uniformly within the spawning zones for each case. On average, one individual was released in every 0.4 km^2.

Vertically, individuals were released at the bottom of the water column where spawning occurs. Their subsequent vertical motion was driven by vertical diffusion and advection. Individuals were released at a frequency of 6 h following a Gaussian distribution during the 10-d spawning period. This scheme is based on the assumption that multiple spawning peaks may occur within a spawning season (Tettelbach *et al*., 1999) and that peak spawning occurs towards the middle of this 10-d spawning event.

For each case, a matrix of connectivity, P_{ij}, between spawning zones i and settlement zones j were computed according to the following procedure.

1. In FISCM, larvae were released every 6-h over 10 d following a normal temporal distribution. The IBM was run for 24 days which included 10 days for the spawning event and 14 days for the maximum LPD.
2. For each spawning zone, a LPDF [$f_{\psi}(\vec{x}, \tau)$] and a settlement PDF [$F_{\Psi}(\vec{x})$] (Eqs. (5) and (6)) were calculated.
3. The settlement PDF of a given spawning zone was integrated over the area of each settlement zone to give the connectivity (P_{ij}) from spawning zone i to settlement zone j.

Settlement success metrics

Settlement success metrics were defined based on connectivity matrices. A Zone Settlement Success (ZSS_i), defined as the overall settlement success of larvae from a particular spawning zone, i, was calculated by summing the settlement zone (column) elements of the connectivity matrix, j:

$$ZSS_i = \sum_j P_{ij} \tag{9}$$

Also determined was an Average Zone Success (*AZS*), taken as the arithmetic mean of *ZSS* over all spawning zones. This serves as a bay-wide score for settlement success for a given spawning event.

RESULTS

Circulation

The fields of model-generated velocity averaged vertically and over the time span of each realistic spawning event, together with corresponding volume transport stream function fields, show a number of common flow features (Fig. 4).

One is a bi-directional pattern in the large-scale flow field, driven by the dominant southwesterly wind forcing, in which the flow in shallow (depth < ~ 10 m) nearshore areas is directed up-bay (along the wind) and the flow in deeper areas of the bay interior is directed down-bay (against the wind). This pattern, especially evident in the upper bay, is consistent with the modeled response of the bay to an idealized SW sea breeze (Liu, 2014) as well as with the modeling results of Signell (1987). The fundamental dynamics of such a bi-directional response to along-shore wind forcing were first described by Csanady (1973) in the study of long lakes.

Eddies with length scales from 1 to 8 km are also evident in the mean circulation. Prominent eddies appear near the openings of Woods Hole, Quicks Hole and Cape Cod Canal (Fig. 2). They appear to be due to tidal rectification as they are present in the circulation of the model run forced by M_2 tide only (Case I1; Liu, 2014).

The similarity of mean flows for the six spawning events may be due to the small variation in observed winds and tides. The consistency of the winds over Buzzards Bay is typical of most summers. Analysis of the BUZM3 wind record reveals little interannual

variation in the wind properties during the spawning periods of 2001 to 2010. Spawning-period winds of all years are SW-dominant with prevailing directions between 200° and 250° (Table 1).

Connectivity for realistic cases

Connectivity matrices for the six realistic cases (Fig. 5) exhibit some common patterns. For all cases, the highest connectivities fall along the matrix diagonal, i.e. in the matrix elements representing self-connectivity. Strong self-connectivities with small case-to-case variation are indicated for zones in which both spawning and settlement areas have limited exposure to open bay waters. The most notable example is zone 1 (Westport River, with P_{ii} of 0.33-0.39), followed by zones 20 (Canal bays, 0.16-0.19), 19 (Wareham harbors, 0.11-0.15) and 3 (Slocums River, 0.11-0.13). High, but more widely varying, self-connectivities are indicated for zones in which spawning and settlement have greater exposure to open bay currents, including zones 4 (Apponagansett Harbor, 0.14-0.28), 7 (New Bedford Harbor, 0.04-0.16), 9 (Nasketucket Bay, 0.08-0.16), 14 (Mattapoisett Harbor, 0.04-0.13) and 16 (Sippican Harbor, 0.19-0.37). Consistently low (<0.01) self-connectivity is indicated for those zones with spawning areas in the open bay (zones 6, 8, 11, 13, 15, 17 and 23).

The connectivities between different spawning and settlement zones (cross-connectivities) exhibit a pattern consistent with the mean sea breeze-driven circulation of Buzzards Bay. For spawning zones along the western bay (1-19), non-zero connectivities predominantly fall below the diagonal of the connectivity matrix, indicating successful larval transport to higher number settlement zones further up-bay (carried by the nearshore up-bay mean circulation indicated in Fig. 4). Similarly, non-zero connectivities of

spawning zones of the eastern bay (21-25) are predominately above the matrix diagonal, to lower number settlement zones, also indicative of up-bay larval transport.

This pattern where larval transport is predominately directed to up-bay settlement areas is reflected in the connectivities averaged over bay region (Fig. 6). The largest averaged connectivies (>0.0330) are between mid- and eastern-bay spawning areas and settlement areas in the upper-bay. A somewhat smaller (0.0068) connectivity is indicated for larval transport from lower-bay spawning to mid-bay settlement. Very small probabilities (<0.0025) of down-bay spawning-to-settlement region transport are also indicated.

To assess how the spawning-to-settlement area connectivity varies with year and stage of the spawning season, linear regression analysis relating the connectivities of all possible pairs of the six the realistic cases were performed. The correlations of the cross- and self-connectivities of the various pairs are presented separately (Table 3, Fig. 7). These have been distinguished because case-to-case differences of cross-connectivity predominately reflect temporal variations in Buzzards Bay circulation, whereas temporal differences in self-connectivity are more closely tied with variations in embayment circulation. Furthermore, self-connectivities reach significantly higher values than cross-connectivities (Fig. 5), and thus tend to dominate case-to-case correlations and mask the relation between the cross-connectivities of different cases.

The self-connectivities of the realistic cases were strongly correlated, with R^2 >0.85 (and predominately ≥0.90) (Table 3a). The case-to-case correlations of the cross-connectivities were weaker, with R^2 as low as 0.61 (Table 3b). Importantly, the slopes of the linear regression lines relating both the self- and cross-connectivies of the realistic cases do not differ appreciably from unity, ranging between 0.70 and 1.12 (Table 3), implying that there are no cases where the modeled currents give either self- or cross-connectivities

that are unusually high or low, compared with all other cases, over the entire bay. However, as noted above, there were zones where the self-connectivities vary considerably from case to case (Fig 7a). Individual cross-connectivities also show considerable case-to-case variation as indicated by the broad scatter of the cross-connectivities of one case plotted against another (Fig 7b).

Impact of tides and wind on dispersal and connectivity

The results of Case I1 demonstrate that when carried by tidal and tidally-forced currents only, individuals tend to be retained in the spawning zones where they were released (Fig. 8a). The extent of the transport of individuals was limited to the neighboring settlement zones, usually within 12 km of their source. The largest spawning-to-settlement zone excursions due to tidally-forced currents are seen in the mid-bay region (Fig. 8a). For this region, high levels of connectivity occur above the diagonal of the connectivity matrix, indicating successful larval transport from spawning areas to settlement zones further down-bay, counter to the nearshore sea breeze-driven circulation discussed above.

The connectivity matrices for Cases I2 (constant SW wind) and I3 (idealized sea breeze) exhibit a far greater level of larval dispersal than displayed by the connectivity matrix of Case I1 (Fig. 8). The addition of the SW wind forcing generates a nearshore downwind flow that dominates the tidally-driven flow in transporting larvae and results in cross-connectivity predominately between spawning areas and settlement zones further up-bay (i.e., as indicated by connectivities below the matrix diagonal for spawning zones 1-19, and above the diagonal for spawning zones 21-25). Up-bay larval excursions of Case I2 exceed those of Case I3 and result in connectivities spanning the length of Buzzards Bay (i.e., from spawning zone 2 to settlement zone 19). The geographic extent of the cross-connectivities

of Case I3 was similar to the geographic reach of the cross-connectivities of the realistic cases (Figs. 5 and 8c), an indication that the sea breeze-driven circulation is the dominant factor in producing the connectivity patterns of the realistic cases.

The mean vertically-averaged velocity field of Case I4 (Fig. 9), driven by NW-dominant (cross-bay) winter winds, shows a number of prominent features not apparent in the mean velocity fields driven by the winds of the summer spawning period (Fig. 4). These features include a strong down-bay flow along the eastern shore and anticyclonic eddies extending across the bay in the upper- and mid-bay regions. The connectivity matrix of Case I4 (Fig. 8d) shows a more even distribution of non-zero connectivities above and below the diagonal than observed in the connectivity matrices of the realistic cases (Fig. 5). The implication is that if larvae were spawned in the winter period, they would experience both up- and down-bay transport to settlement areas, with a much higher probability of being carried to down-bay settlement areas than larvae spawned in the summer period.

Settlement Success Metrics

In judging the effectiveness of spawning areas as suppliers of settlement-capable larvae to juvenile habitat (areas with bottom depth <3.5 m) we computed two versions of *ZSS*. One, ZSS_{all}, included all settlement zones in the summation (Eq. 9) (i.e., summing over self-connectivity and cross-connectivities for a given spawning zone). The second, ZSS_{cc}, included only cross-connectivity in the summation (more fully reflecting the influence of bay currents on larval delivery to settlement areas).

The ZSS_{all} scores for the six realistic cases (Fig. 10a) were dominated by high values (>0.16) for five spawning zones (1, 4, 9, 16 and 20), all of which have spawning and settlement areas deep within an embayment. The ZSS_{cc} have high values distributed over a

greater number of spawning zones (Fig. 10b) and exhibit more case-to-case variability for a given zone than ZSS_{all}.

An ANOVA was performed to evaluate the degree of similarity in *ZSS* over the six realistic cases. *ZSS* were arcsine-square-root-transformed, to meet the assumptions of ANOVA (Sokal and Rohlf, 1995). The results indicate that ZSS_{all} of the six realistic spawning cases are highly similar (p=0.968), suggesting that bay-wide settlement success is stable over years and spawning seasons. Nevertheless, there were large variations in ZSS_{all} for some spawning zones, exceeding a factor of 2 for eight zones. ANOVA shows much higher case-to-variation of ZSS_{cc} (p = 0.871). ZSS_{cc} variations exceed a factor of 2 for 13 spawning zones and are greater than a factor of 4 for four zones.

From averages of ZSS_{all} over the realistic cases ($<ZSS_{all}>$, see Fig. 11), we may define two classes of spawning zones, those from which larvae have little probability of successful settlement ($<ZSS_{all}>$ <0.05) and those from which larvae have a modest to high probability of settlement ($<ZSS_{all}>$ >0.075; no $<ZSS_{all}>$ fall in the 0.05-0.075 range). Zones in the former class (2, 13, 15, 17, 23 and 25) all have spawning areas within the open bay (Fig. 3). Zones in the latter class, may be further divided into three categories, those in which $<ZSS_{all}>$ is: 1) principally due to self-connectivity ($<ZSS_{cc}>/<ZSS_{all}>$ <0.3; zones 1, 3, 4, 7, 16, 19, 20 and 21), 2) due to a mix of cross- and self-connectivity ($0.3 \leq <ZSS_{cc}>/<ZSS_{all}>$ <0.7; zones 9, 14, 22 and 24) and largely due to cross-connectivity ($<ZSS_{cc}>/<ZSS_{all}> \geq 0.7$; zones 5, 6, 8, 10, 11, 12 and 18).

The levels of average zone success (*AZS*) vary little over the six realistic cases, ranging from 0.11 to 0.14 (Table 4; Fig. 12), indicating that no case stands out as being particularly favorable for spawning-to-settlement zone connectivity on a bay-wide basis.

Sensitivity experiments

The results of IBM experiments should be independent of the number of individuals released. To test the sensitivity to the number of individuals released, we repeated the 2008 early spawning case (R1) but increased the density of release sites from one per 0.4 km^2 to one per 0.2 km^2, raising the total number of individuals released from 47,631 to 95,262. The connectivity matrix derived from the larger number of simulated tracks differed only slightly from the matrix of the original simulation. The root mean square difference of the two connectivity matrices was only 0.25%.

We also conducted a sensitivity experiment to examine the dependence of the results on the IBM time step. We repeated the 2008 early spawning case (R1) but with a 120-s IBM time step, half that of the original simulation. The root mean square difference between the resulting connectivity matrix and that of the original simulation was only 0.4%.

Tests were conducted to assess the sensitivity of the results to the IBM scheme employed for particles crossing the horizontal boundary. In FISCM, an individual crossing a solid horizontal boundary was placed back to its last in-domain location. We tested another boundary crossing approach in which an individual crossing a boundary edge is placed at the midpoint between the centroid of the cell where it last resided and its last valid location. The root mean square difference for the connectivity matrices of the two cases having different lateral boundary conditions was 0.82%.

DISCUSSION

Spawning in Buzzards Bay occurs during a time when the wind forcing is dominated by the seasonal sea breeze. Being largely wind-driven (Signell, 1987), the bay-scale circulation thus varies relatively little during and between spawning seasons. As a result, the IBM

model results do not show large season-to-season or intra-seasonal differences in bay-wide spawning-to-settlement-zone connectivity. Most importantly, no year stands out as one in which bay-wide connectivity is particularly high. This is in contrast with the large variation in yearly scallop harvest from Buzzards Bay recorded during our study period (Fig. 12). On first consideration, one may conclude that variations in spawning-to-settlement-area connectivity have very little impact on the overall population of scallops in Buzzards Bay. However, for any given year, scallop spawning is not likely to be uniformly distributed over the designated spawning areas of our model. In addition, conditions for juvenile scallop health in settlement areas are likely to vary. Our results have demonstrated that the connectivity between specific spawning zones and suitable juvenile habitat can have a sizeable seasonal and year-to-year variation. If such zones are principal centers of spawning, then a large annual variation in connectivity may be expected. Large annual variations in connectivity may also result from year-to-year shifts in the principal areas of spawning activity, i.e., to and from areas with markedly different connectivity with suitable juvenile habitat. For all realistic cases, the connectivity of spawning zones with juvenile habitat (ZSS_{all}) varies by an order of magnitude (Table 4). As an extreme example, the bay-wide settlement success for the case where all of the larvae are released in zone 1 ($<ZSS_{all}>=0.35$) versus one where all larvae are released from zone 17 ($<ZSS_{all}>=0.04$) differs by a factor of 10. These differences can be further amplified when considering biological factors such as the positive influence of spawning density on fertilization success (e.g. Tettelbach *et al.*, 2013; Hall, 2014). Such coupling can contribute to the three orders of magnitude in variation in catch observed over the five-year period from 2007-2012 (Fig. 12).

Temperature has an influence on larval duration and thus has the potential to impact dispersion. For this subspecies of bay scallop, the PLD can be as short as 6-8 days when reared at optimal conditions (23.2 °C; Tettelbach & Rhodes, 1981) and 14 days or longer at less than optimal conditions. To consider the potential influence of temperature variation in the three years of modeled spawning seasons, statistics from a long-term local observation in Woods Hole, MA were computed. For the three years modeled in this work (2008-2010), the temperature range during the spawning period in 2009 was slightly colder (15.9 ~ 22.8 °C) when compared with the other two years (18.1 ~ 22.6 °C). In the context of the the influence of temperature on larval growth and survival rate (Tettelbach and Rhodes, 1981), the relatively small interannual variation in Buzzards Bay water temperature is not likely sufficient enough to strongly influence the larval duration and therefore the settlement success.

Field studies on bay scallop larval settlement in other parts of the eastern USA suggest that tidally-induced circulation is the dominant mechanism of larval transport (Peterson et al., 1996; Arnold *et al*., 1998; Marko & Barr, 2007; Tettelbach *et al.*, 2013) whereas the wind-driven circulation is not significant (Peterson *et al.*, 1996; Tettelbach *et al.*, 2013). This was also an inherent assumption of the Lagrangian particle tracking study on bay scallop larvae conducted by Siddall *et al.* (1986) where only tidal forcing is included in the hydrodynamic model. However, in Buzzards Bay, the sea breeze is the dominant forcing mechanism for the subtidal circulation during spawning season. The idealized cases conducted in the present effort indicated that larval connectivity would be significantly different if wind forcing were excluded. Therefore, to model bay scallop larval transport and connectivity in Buzzards Bay, a comprehensive hydrodynamic model that includes both tidal and wind forcing is necessary.

The designation of *ZSS* scores may be useful to fisheries managers in targeting areas for spawning enhancement measures, i.e., planting scallops or limiting scallop harvest. For example, if a principal aim is to increase local scallop production, enhancement efforts may be directed at the zones in category 1 with the highest $<ZSS_{all}>$, in particular zones: 1 (Westport River, $<ZSS_{all}>$ = 0.33), 4 (Apponagansett Harbor, 0.26), 16 (Sippican harbor, 0.30) and 20 (Canal Bays, 0.19). Conversely, a zone in category 1 may not be considered as priority for enhancement, despite a high $<ZSS_{all}>$ score, if its environment is deemed of poor quality for scallop growth, as enhancement measures in such a zone will likely have limited benefits beyond the zone. A category 2 zone with high $<ZSS_{all}>$ may be considered as high priority for enhancement operations if these are aimed at increasing scallop production within the zone and over a broader region. Top $<ZSS_{all}>$ zones in category 2 are: 9 (Nasketucket Bay, 0.20) and 14 (Mattapoisett Harbor, 0.13). Finally, zones in category 3 with high $<ZSS_{all}>$ may considered ideal for enhancement measures aimed at increasing production over a broad region, particularly if such measures can be implemented with minimal disruption to scallop harvesting (i.e., due to lack of easy access for scalloping in the target zone). The $<ZSS_{all}>$ scores of category 3 zones are narrowly distributed, falling between 0.11 and 0.13 for all but one zone (11).

The model did not incorporate all of those processes which may contribute to temporal variations in connectivity. In particular, the hydrodynamic model neglected fresh water runoff. Variations in runoff may result in appreciable changes in circulation, and larval transport, within rivers and embayments, areas of particularly high self-connectivity. Vertical swimming larvae has been shown to influence larval dispersion (North et al., 2008; Tian et al., 2009b; Gilbert et al., 2010), particularly in areas of strong tides and/or estuarine

circulation (Forward and Tankersley, 2001). Due to a paucity of information on the vertical swimming behavior of scallop larvae, such behavior was not included in the simulations. The "individuals" were treated as passive particles and were subject only to vertical diffusion and advection. The IBM model did not account for larval mortality, which can result from starvation, predation or disease, factors that may vary annually with changing conditions in the bay (MacFarlane, 1999). The specification of suitable juvenile habitat as areas with bottom depth < 3.5 m was based on observed abundance of eelgrass distributions in the Bay. However, bay scallop juveniles also attach to macroalgae species which occur at greater depths than eelgrass, such as *Codium fragile* and *Spyridia filamentosa*. Inclusion of settling to these deeper habitats could influence the computation of settlement success but was not considered in this effort due to lack of information regarding macroalgae distributions.

The health of scallop populations in Buzzards Bay are sensitive to a range of environmental conditions. Turner *et al.* (2009) found that the biomass of diatoms and microflagellates, principal elements of the bay scallop diet, is highly variable, both seasonally and interannually. The Buzzards Bay Coalition has used data on nitrogen (organic and inorganic), water clarity, dissolved oxygen, and algal pigments acquired since 1992 to derive a health index of the bay and its embayments (http://www.savebuzzardsbay.org/BayHealthData). The index for many locations shows significant annual variations, up to an order of magnitude, which will likely impact local scallop populations.

While our study has provided useful insight into those processes affecting spawning-to-settlement connectivity in Buzzards Bay, further understanding of scallop population dynamics in the bay will require more advanced observational and modeling studies directed at the full range of processes impacting scallop recruitment and growth.

ACKNOWLEDGEMENTS

The authors would like to thank the reviewers for their valuable comments and suggestions which did much to improve the manuscript. Thanks to Valerie Hall and Stephen Tettelbach for their input on bay scallop biology. Thanks to Brant McAfee (Massachusetts Division of Marine Fisheries), Joe Costa (Buzzards Bay National Estuary Program), and Rich Signell (U.S. Geological Survey) who provided data used in this work. This project was supported by the Woods Hole Sea Grant through award NA10OAR4170083. All modeling computations were made on the University of Massachusetts at Dartmouth's (UMD's) GPGPU cluster, which was acquired with support from NSF award CNS-0959382 and AFOSR DURIP award FA9550-10-1-0354. This paper is #13-0801 in the School for Marine Science and Technology (UMD) Contribution Series.

REFERENCES

Arnold W.S., Marelli D.C., Bray C.P., Harrison M.H. (1998) Recruitment of bay scallops *Argopecten irradians* in Floridan Gulf of Mexico waters: scales of coherence. *Marine Ecology Progress Series* **170**:143–157.

Banas, N., McDonald, P., and Armstrong, D. (2009) Green crab larval retention in Willapa Bay, Washington: An intensive Lagrangian modeling approach. *Estuaries and Coasts* **32**: 893–905. 10.1007/s12237-009-9175-7.

BBNEP (2012) *Composite map of current eelgrass distribution (2001-2010) datalayer*. Published by Buzzards Bay National Estuary Program, East Wareham, MA, USA. `http://buzzardsbay.org/eelgrass-historical.htm`.

Belding, D.L. (1910) A report upon the scallop fishery of Massachusetts: Including the habits, life history of *Pecten irradians*, its rate of growth, and other facts of economic value. Technical report, Massachusetts Commissioners on Fisheries and Game, 150 pp.

Belding, D.L. (1931) The scallop fishery of Massachusetts. Technical report, Massachusetts Commissioners on Fisheries, 48 pp.

Bishop M.J., Rivera J.A., Irlandi E.A., Ambrose W.G. Jr, Peterson C.H. (2005) Spatio-temporal patterns in the mortality of bay scallop recruits in North Carolina: investigation of a life history anomaly. *Journal of Experimental Marine Biology and Ecology* **315**(2):127–146.

Blake, N.J. and Shumway, S.E. (2006) Bay scallop and calico scallop fisheries, culture and enhancement in eastern North America. In S.E. Shumway and G.J. Parsons, (eds.), *Scallops: Biology, Ecology and Aquaculture*, Elsevier, volume 35, chapter 17, pages 945–964.

Botev, Z., Grotowski, J., and Kroese, D. (2010) Kernel density estimation via diffusion. *The Annals of Statistics* **38**(5): 2916–2957.

Boucher, J.M., Chen, C., Sun, Y., and Beardsley, R.C. (2013) Effects of interannual environmental variability on the transport-retention dynamics in haddock *Melanogrammus aeglefinus* larvae on Georges Bank. *Marine Ecology Progress Series* **487**: 201–215.

Bricelj, V.M., Epp, J., and Malouf, R.E. (1987) Intraspecific variation in reproductive and somatic growth cycles of bay scallops *Argopecten irradians*. *Marine Ecology Progress Series* **36**: 123–137.

Carroll, J.M., Peterson, B.J., Bonal, D., Weinstock, A., Smith, C.F., and Tettelbach, S.T. (2010) Comparative survival of bay scallops in eelgrass and the introduced alga, *Codium fragile*, in a New York estuary. *Marine Biology* **157**(2): 249–259.

Chen, C., Beardsley, R., and Cowles, G. (2006) An unstructured grid finite-volume coastal ocean model system. *Oceanography* **19**(1): 78–89.

Chen, C., Huang, H., Beardsley, R.C., Xu, Q., Limeburner, R., Cowles, G., Sun, Y., Qi, J., and Lin, H. (2011) Tidal dynamics in the Gulf of Maine and New England Shelf: An application of FVCOM. *Journal of Geophysical Research* **116**(C12010).

Chen, C., Liu, H., and Beardsley, R.C. (2003) An unstructured grid, finite-volume, three-dimensional primitive equation ocean model: Application to coastal ocean and estuaries. *Journal of Atmospheric and Oceanic Technology* **20**: 159–186.

Chen, C., Qi, J., Li, C., Beardsley, R.C., Lin, H., Walker, R., and Gates, K. (2008) Complexity of the flooding/drying process in an estuarine tidal-creek salt-marsh system: An application of FVCOM. *Journal of Geophysical Re- search: Oceans* **113**(C7).

Churchill, J.H., Runge, J., and Chen, C. (2011) Processes controlling retention of spring-spawned Atlantic cod (*Gadus morhua*) in the western Gulf of Maine and their relationship to an index of recruitment success. *Fisheries Oceanography* **20**(1): 32–46. 10.1111/j.1365-2419.2010.00563.x.

Costello, C. and Kenworthy, W. (2011) Twelve-year mapping and change analysis of eelgrass (*Zostera marina*) areal abundance in Massachusetts (USA) identifies statewide declines. *Estuaries and Coasts* **34**(2): 232–242. 10.1007/s12237-010-9371-5.

Cowles, G.W. (2008) Parallelization of the FVCOM coastal ocean model. *International Journal of High Performance Computing Applications* **22**(2): 177–193.

Cowles, G., Lentz, S., Chen, C., Xu, Q., and Beardsley, R. (2008) Comparison of observed and model-computed low frequency circulation and hydrography on the New England shelf. *Journal of Geophysical Research* **113**(C9): C09015. 10.1029/2007JC004394.

Csanady, G.T. (1973) Wind-induced barotropic motions in long lakes. *Journal of Physical Oceanography* **3**(4): 429–438.

FISCM (2013) FVCOM I-State Configuration Model (FISCM) Source Code. https://github.com/GeoffCowles/fiscm.

Forward Jr., R.B and Tankersley, R.A. (2001) Selective tidal-stream transport of marine animals. *Oceanography and Marine Biology: An Annual Review* **39**:305-353.

Gilbert, C., Gentleman, W., Johnson, C., DiBacco, C., Pringle, J., and Chen, C. (2010) Modelling dispersal of sea scallop (*Placopecten magellanicus*) larvae on Georges Bank: The influence of depth-distribution, planktonic duration and spawning seasonality. *Progress in Oceanography* **87**(1–4): 37 – 48. 10.1016/j.pocean.2010.09.021.

Ji, R., Ashjian, C.J., Campbell, R.G., Chen, C., Gao, G., Davis, C.S., Cowles, G.W., and Beardsley, R.C. (2011) Life history and biogeography of calanus copepods in the Arctic Ocean: An individual-based modeling study. *Progress In Oceanography* **96**(1): 40–56.

Hall V.A. (2014) Impact of the second seasonal spawn on reproduction, recruitment, population and life history of the northern bay scallop. Ph.D. Thesis. University of Massachusetts Dartmouth, Dartmouth, MA.

Kobayashi, M.H., Pereira, J.M.C., and Pereira, J.C.F. (1999) A conservative, finite-volume second order-accurate projection method on hybrid unstructured grids. *Journal of Computational Physics* **150**: 40–45.

Le Pennec, M. (2003). The pelagic life of the pectinid Pecten maximus—a review. *ICES Journal of Marine Science*, **60**(2), 211–223. doi:10.1016/S1054-3139(02)00270-9

Liu, C. (2014). Quantifying connectivity in Buzzards Bay with application to the study of recruitment variability in the bay scallop (*Argopecten irradians*) Master's thesis. University of Massachusetts Dartmouth, Dartmouth, MA.

Loosanoff, V.L. and Davis, H.C. (1963) Rearing of bivalve mollusks. Academic Press, volume 1 of *Advances in Marine Biology*, pages 1–136.

MA DFG (2009) *Designated Shellfish Growing Areas Datalayer — October 2009*. Published by MassGIS (MA Office of Geographic and Environmental Information), Executive Office of Energy and Environmental Affairs, Department of Fish and Game, Division of Marine Fisheries, Boston, MA, USA.

MacFarlane, S. (1999) Bay scallops in Massachusetts waters: A review of the fishery and prospects for future enhancements and aquaculture. Technical report, Barnstable County's Cape Cod Cooperative Extension and Southeastern Massachusetts Aquaculture Center.

MacKenzie, C. (2008) The bay scallop, *Argopecten irradians*, Massachusetts through North Carolina: Its biology and the history of its habitats and fisheries. *Marine Fisheries Review* **70**: 6–79.

Marko P.B., Barr K.R. (2007) Basin-scale patterns of mtDNA differentiation and gene flow in the bay scallop *Argopecten irradians concentricus*. *Marine Ecology Progress Series* **349**:139–150.

McNamara M.E., Lonsdale D.J., Cerrato R.M. (2010) Shifting abundance of the ctenophore *Mnemiopsis leidyi* and the implications for larval bivalve mortality. *Marine Biology* **157**:401–412.

Mitarai, S., Siegel, D., Watson, J., Dong, C., and McWilliams, J. (2009) Quantifying connectivity in the coastal ocean with application to the Southern California Bight. *Journal of Geophysical Research* **114**: C10026. Doi:10.1029/2008JC005166.

NeCOFS (2013) Northeast Coastal Ocean Forecasting System (NeCOFS) Main Portal. `http://fvcom.smast.umassd.edu/research_projects/NECOFS`.

North, E., Schlag, Z., Hood, R., Li, M., Zhong, L., Gross, T., and Kennedy, V. (2008) Vertical swimming behavior influences the dispersal of simulated oyster larvae in a coupled particle-tracking and hydrodynamic model of Chesapeake Bay. *Marine Ecology Progress Series* **359**: 99–115.

Peterson C.H., Summerson H.C., Luettich R.A. Jr (1996) Response of bay scallops to spawner transplants: a test of recruitment limitation. *Marine Ecology Progress Series* **102**:93–107.

Petrik, C. (2011) Modeling the processes affecting larval haddock (*Melanogrammus aeglefinus*) survival on Georges Bank. Ph.D. thesis, Massachusetts Institute of Technology, Cambridge, MA.

Roughan, M., Macdonald, H.S., Baird, M.E., and Glasby, T.M. (2011) Modelling coastal connectivity in a western boundary current: Seasonal and inter-annual variability. *Deep Sea Research Part II: Topical Studies in Oceanography* **58**(5): 628–644. 10.1016/j.dsr2.2010.06.004.

Sastry, A. (1965) The development and external morphology of pelagic larval and post-larval stages of the bay scallop, *Aequipecten irradians concentricus* Say, reared in the laboratory. *Bulletin of Marine Science* **15**(2): 417–435.

Siddall S.E., Vieira M.E., Gomez-Reyes E, Pritchard D.W. (1986) Numerical model of larval dispersion. Special Report No. 71, Marine Science Research Center, Stony Brook, NY.

Siegel, D.A., Mitarai, S., Costello, C.J., Gaines, S.D., Kendall, B.E., Warner, R.R., and Winters, K.B. (2008) The stochastic nature of larval connectivity among nearshore marine populations. *Proceedings of the National Academy of Sciences of the United States of America* **105**(26): 8974–8979.

Signell, R.P. (1987) Tide- and wind-forced currents in Buzzards Bay, Massachusetts. Master's thesis, Massachusetts Institute of Technology, Cambridge, MA.

Sinclair, M. (1988) *Marine Populations: An Essay on Population Regulation and Speciation.* Seattle, WA: University of Washington Press.

Sokal, R. and Rohlf, F. (1995) *Biometry*. New York: W. H. Freeman and Company, third edition.

Taylor, R. and Capuzzo, J. (1983) The reproductive cycle of the bay scallop, *Argopecten irradians irradians* (Lamarck), in a small coastal embayment on Cape Cod, Massachusetts. *Estuaries* **6**(4): 431–435. 10.2307/1351403.

Tettelbach S.T., Peterson B.J., Carroll J.M., Hughes S.W.T., Bonal D.M., Weinstock A.J., Europe J.R., Furman B.T., Smith C.F. (2013) Priming the larval pump: resurgence of bay scallop recruitment following initiation of intensive restoration efforts. *Marine Ecology Progress Series* **478**:153–172.

Tettelbach S.T., Rhodes E.W. (1981) Combined effects of temperature and salinity on embryos and larvae of the northern bay scallop, *Argopecten irradians irradians*. *Marine Biology* **63**(3):249–256.

Tettelback, S. T., Smith, C. F., Smolowitz, R., Tetrault, K., & Dumais, S. (1999). Evidence for fall spawning of northern bay scallops *Argopecten irradians irradians* (Lamarck 1819) in New York. *Journal of Shellfish Research*, **18**(1), 47–58.

Tettelbach S.T., Wenczel P., Hughes S.W.T. (2001) Size variability of juvenile (0+ Yr) bay scallops, *Argopecten irradians irradians* (Lamarck, 1819) at eight sites in Eastern Long Island, New York. *Veliger* **44**(4):389–397.

Thayer, G. and Stuart, H. (1974) The bay scallop makes its bed of seagrass. *Marine Fisheries Review* **36**(7): 27–30.

Tian, R., Chen, C., Stokesbury, K., Rothschild, B., Cowles, G., Xu, Q., Hu, S., Harris, B., and II, M.M. (2009a) Dispersal and settlement of sea scallop larvae spawned in the fishery closed areas on georges bank. *ICES Journal of Marine Science* **66**: 2155–2164.

Tian, R., Chen, C., Stokesbury, K., Rothschild, B., Cowles, G., Xu, Q., Hu, S., Harris, B., and II, M.M. (2009b) Dispersal and settlement of sea scallop larvae spawned in the fishery closed areas on georges bank. *ICES Journal of Marine Science* **66**: 2155–2164.

Turner, J.T., Borkman, D.G., Lincoln, J.A., Gauthier, D.A., and Petitpas, C.M. (2009) Plankton studies in Buzzards Bay, Massachusetts, USA. VI. Phytoplankton and water quality, 1987 to 1998. *Marine Ecology Progress Series* **376**: 103–122.

Visser, A. (1997) Using random walk models to simulate the vertical distribution of particles in a turbulent water column. *Marine Ecology Progress Series* **158**: 275–281.

Xue, H., Incze, L., Xu, D., Wolff, N., and Pettirew, N. (2008) Connectivity of lobster populations in the coastal Gulf of Maine. Part I. Circulation and larval transport potential. *Ecological Modelling* **210**: 193–211.

TABLES

Table 1. Coupled biophysical model runs for connectivity experiments. *R* indicates realistic and *I* indicates idealized.

Case	Description
R1	2008 early spawning
R2	2008 later spawning
R3	2009 early spawning
R4	2009 later spawning
R5	2010 early spawning
R6	2010 later spawning
I1	M_2 only, no wind
I2	M_2+constant SW wind
I3	M_2+idealized SW sea breeze
I4	Winter wind forcing

Table 2. Angular wind statistics for realistic cases. Prevailing wind direction is the most frequently occurring wind direction, determined from the wind roses. Wind directions are those from which the winds originate and are in degrees clockwise from north.

Case	Prevailing wind direction	Mean of wind direction	Angular standard deviation
R1 (2008 early)	220/SW	207.8/SSW	50.4
R2 (2008 later)	230/SW	219.2/SW	60.7
R3 (2009 early)	250/WSW	229.8/SW	64.7
R4 (2009 later)	250/WSW	237.4/WSW	52.2
R5 (2010 early)	230/SW	219.5/SW	57.6
R6 (2010 later)	220/SW	192.4/SSW	64.8

Table 3. Squared values of Pearson's correlation coefficient (r^2) and slope of the linear regression line (in square brackets) relating the connectivity levels of each pair of the realistic cases.

Table 3a. Self-connectivity (P_{ii}) correlations (*d.f.*=23).

	R2	R3	R4	R5	R6
R1	0.96 [1.12]	0.92 [0.94]	0.96 [1.09]	0.94 [1.05]	0.95 [0.96]
R2		0.88 [0.80]	0.90 [0.92]	0.92 [0.91]	0.86 [0.79]
R3			0.85 [1.05]	0.98 [1.11]	0.91 [0.96]
R4				0.86 [0.90]	0.96 [0.86]
R5					0.90 [0.86]

Table 3b. Cross-connectivity ($P_{ij}, i \neq j$) correlations (*d.f.*=648).

	R2	R3	R4	R5	R6
R1	0.61 [0.70]	0.69 [0.74]	0.85 [0.87]	0.76 [0.79]	0.83 [0.75]
R2		0.81 [0.90]	0.72 [0.90]	0.86 [0.95]	0.63 [0.73]
R3			0.74 [0.90]	0.80 [0.91]	0.73 [0.78]
R4				0.85 [0.89]	0.91 [0.83]
R5					0.78 [0.79]

Table 4. Summary of ZSS_{all} scores

Case	Min	Mean (*AZS*)	Max
R1 (2008 early)	0.0320	0.1350	0.3316
R2 (2008 later)	0.0261	0.1433	0.3509
R3 (2009 early)	0.0334	0.1340	0.3752
R4 (2009 later)	0.0207	0.1333	0.3998
R5 (2010 early)	0.0094	0.1346	0.3932
R6 (2010 later)	0.0373	0.1198	0.3521

FIGURE CAPTIONS

Figure 1. Landings of bay scallops in Buzzards Bay, Massachuesetts. Source of data: Massachusetts Division of Marine Fisheries and Buzzards Bay National Estuary Program.

Figure 2. Bathymetry (in meters) and unstructured grid for the GoM (regional) and SEMASS (local) nested FVCOM system. Black solid line in the upper panel indicates the boundary between nested grids. The lower panel shows part of the SEMASS grid.

Figure 3. (a) Spawning zones defined using bay scallop suitability areas within designated state shellfish growing areas. (b) Settlement zones defined based on extent of water with depth less than 3.5 m below mean sea level.

Figure 4. Model-computed time- and vertically-averaged velocity field for the six spawning events with forcing by realistic winds (R1-R6). For each case, the average was taken over the duration of each model experiment (from earliest spawning to latest settlement). Vectors in locations where the velocity magnitude is <0.5 cm/s are not rendered. Streamfunctions (in m^3/s) computed using the velocity fields of each case are rendered with white contours. The contour interval is 500 m^3/s.

Figure 5. Connectivity matrices for realistic cases. Elements of each matrix correspond to the settlement success of larval transport from a given spawning zone (the vertical axis) to a given settlement zone (the horizontal axis). Zone numbers are defined in Figs. 3. Dashed horizontal and vertical lines denote larger regions consisting of geographically distinct zones (see text in the *Model experiments* subsection).

Figure 6. Schematic diagram of connectivity pattern among grouped regions representing the average outcome over the six realistic cases. Numbers indicate the connectivity levels for the corresponding spawning-to-settlement regions. Colored regions represent spawning zones. Dashed lines indicate the extent of the 3.5 m isobath containing the settlement zones.

Figure 7. Plots of Case R2 connectivities against Case R6 connectivities, with self- and cross-connectivities plotted in (a) and (b), respectively. Dashed lines represent 1:1 ratios. The least-squares linear fit to the points shown is displayed as a solid line.

Figure 8. Connectivity matrices for the idealized model runs (I1-I4, Table 1). Elements of each matrix correspond to the settlement success of larval transport from a given spawning zone (the vertical axis) to a given settlement zone (the horizontal axis). Zone numbers are defined in Figs. 3. Dashed horizontal and vertical lines denote larger regions consisting of geographically distinct zones (see text in the *Model experiments* subsection).

Figure 9. Same as Fig. 4 except showing the model-computed time- and vertically-averaged velocity field (black arrows) of the spawning event forced by a NW-dominant wind (Case I4). Streamfunctions (in m^3/s) computed using the velocity fields of each case are rendered with white contours. The contour interval is 500 m^3/s.

Figure 10. Zone settlement success (Eq. 9) for the six realistic cases from all 25 spawning zones (Fig. 3a); (a) ZSS_{all}, the settlement success to all settlement zones, (b) ZSS_{cc}, the settlement success without inclusion of self-connectivity.

Figure 11. Geographic map of zone settlement success (ZSS_{all}) averaged over over the six realistic cases.

Figure 12. The AZS (arithmetic mean of ZSS over all spawning zones) of the six realistic cases (a) and commercial bay scallop landings in Buzzards Bay (source: Massachusetts Division of Marine Fisheries) (b). The dashed line box encloses the landings of 2009-2011, which would have been the product of spawning over 2008-2010.

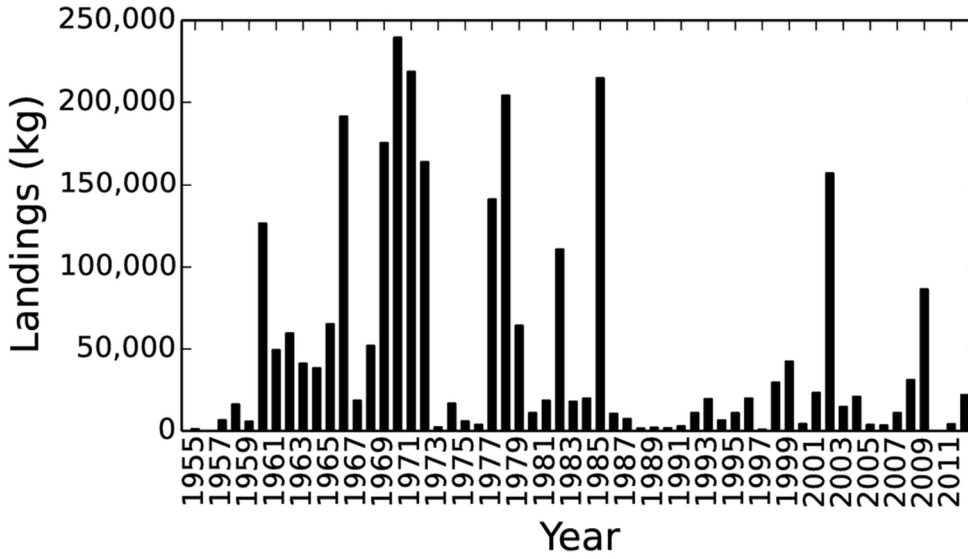

Landings of bay scallops in Buzzards Bay, Massachuesetts. Source of data: Massachusetts Division of Marine Fisheries and Buzzards Bay National Estuary Program.

87x51mm (300 x 300 DPI)

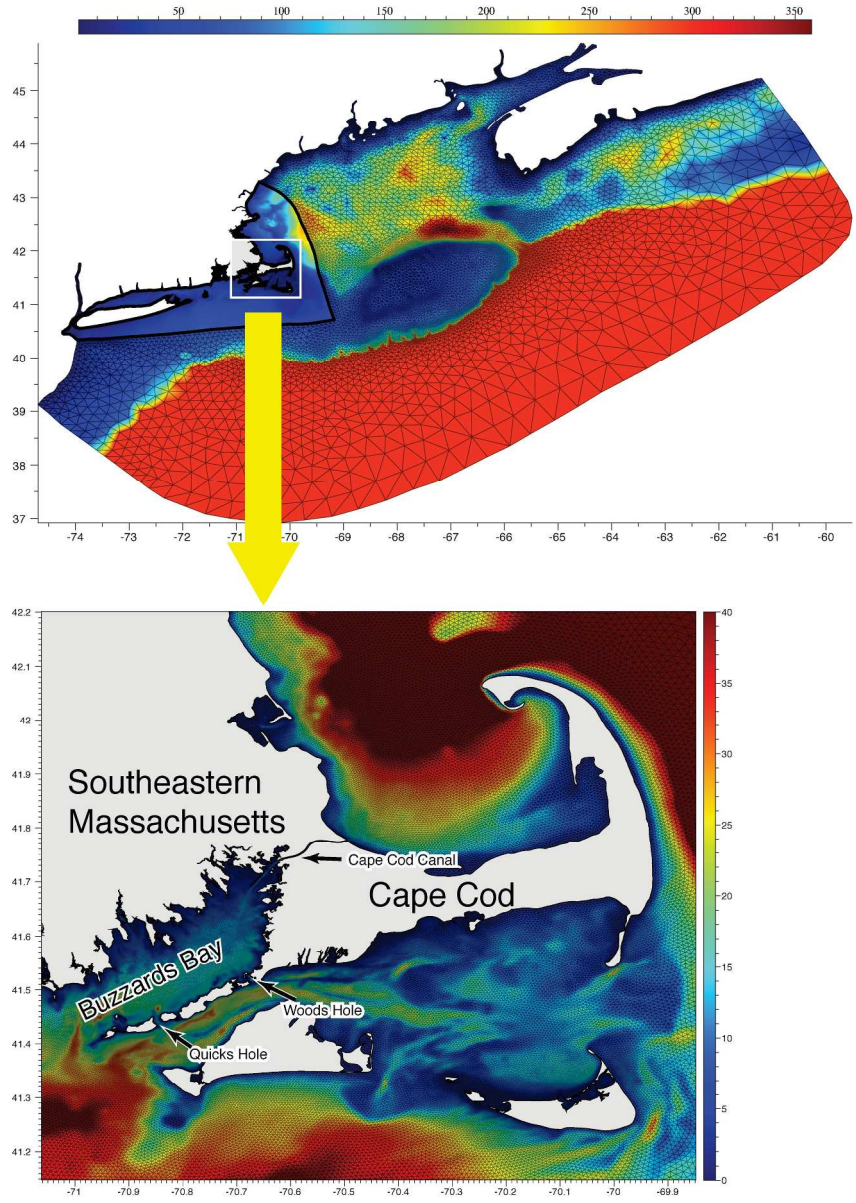

Bathymetry (in meters) and unstructured grid for the GoM (regional) and SEMASS (local) nested FVCOM system. Black solid line in the upper panel indicates the boundary between nested grids. The lower panel shows part of the SEMASS grid.
233x323mm (300 x 300 DPI)

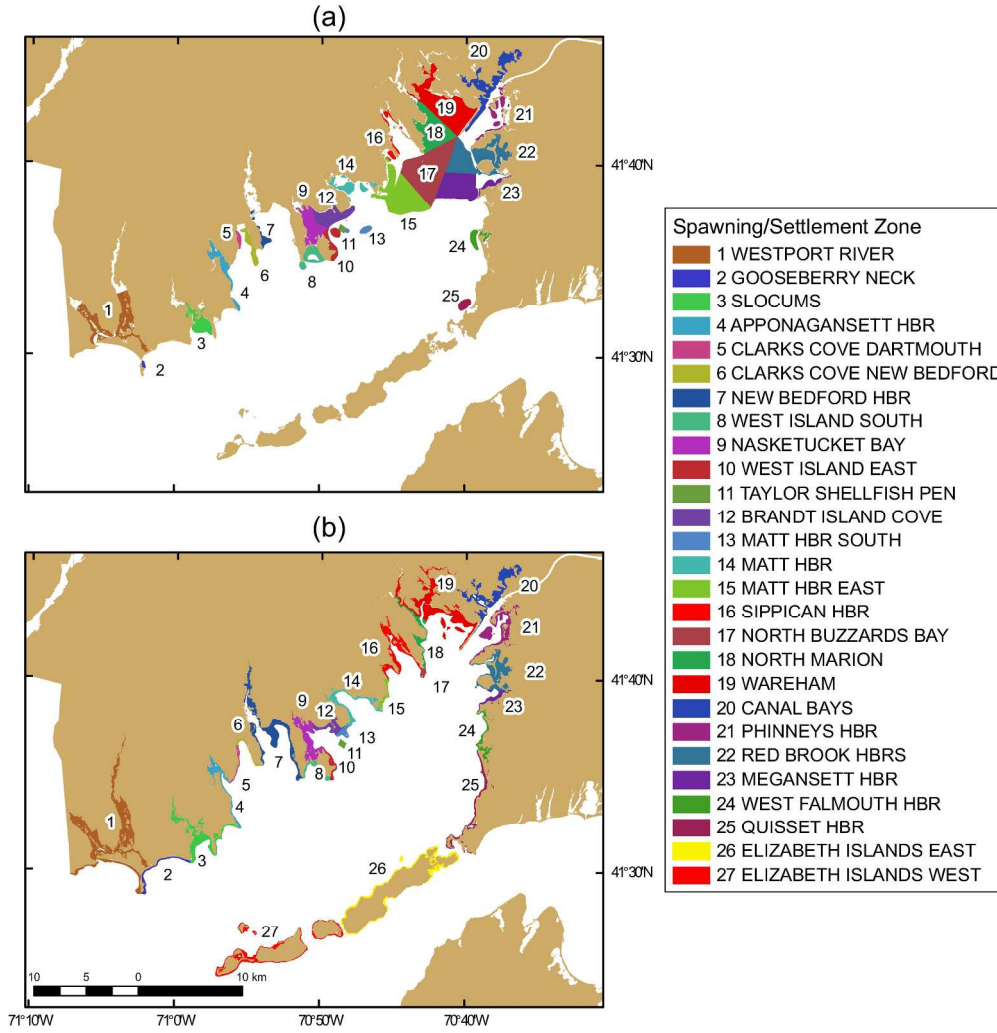

(a) Spawning zones defined using bay scallop suitability areas within designated state shellfish growing areas. (b) Settlement zones defined based on extent of water with depth less than 3.5 m below mean sea level.
272x282mm (300 x 300 DPI)

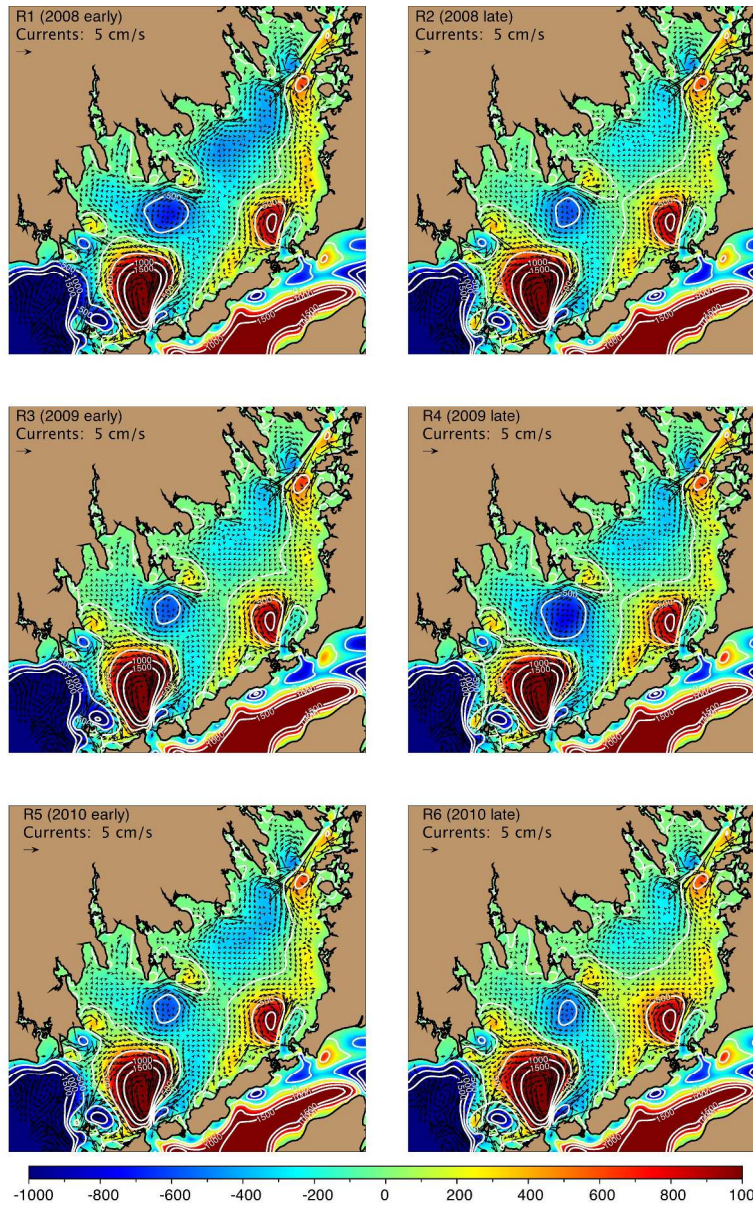

Model-computed time- and vertically-averaged velocity field for the six spawning events with forcing by realistic winds (R1-R6). For each case, the average was taken over the duration of each model experiment (from earliest spawning to latest settlement). Vectors in locations where the velocity magnitude is <0.5 cm/s are not rendered. Streamfunctions
(in m3/s) computed using the velocity fields of each case are rendered with white contours. The contour interval is 500 m3/s.
251x382mm (300 x 300 DPI)

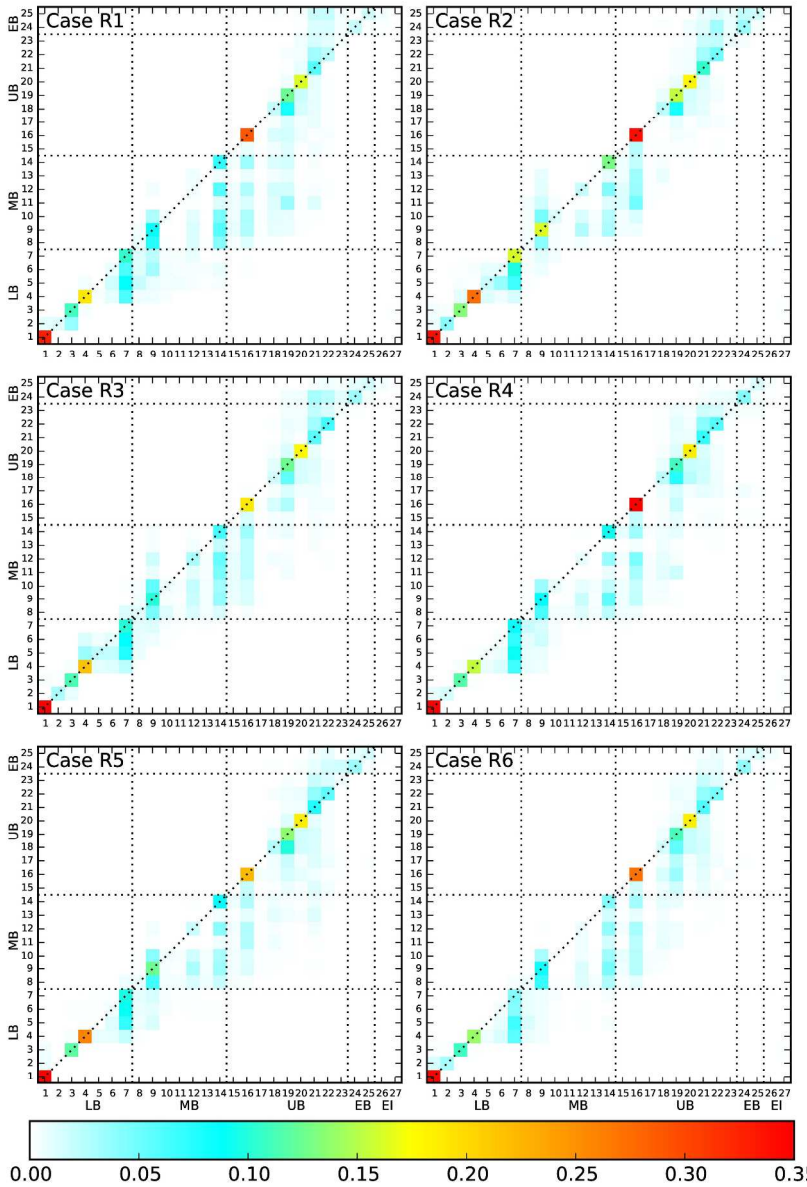

Connectivity matrices for realistic cases. Elements of each matrix correspond to the settlement success of larval transport from a given spawning zone (the vertical axis) to a given settlement zone (the horizontal axis). Zone numbers are defined in Figs. 3. Dashed horizontal and vertical lines denote larger regions consisting of geographically distinct zones (see text in the Model experiments subsection).
264x384mm (300 x 300 DPI)

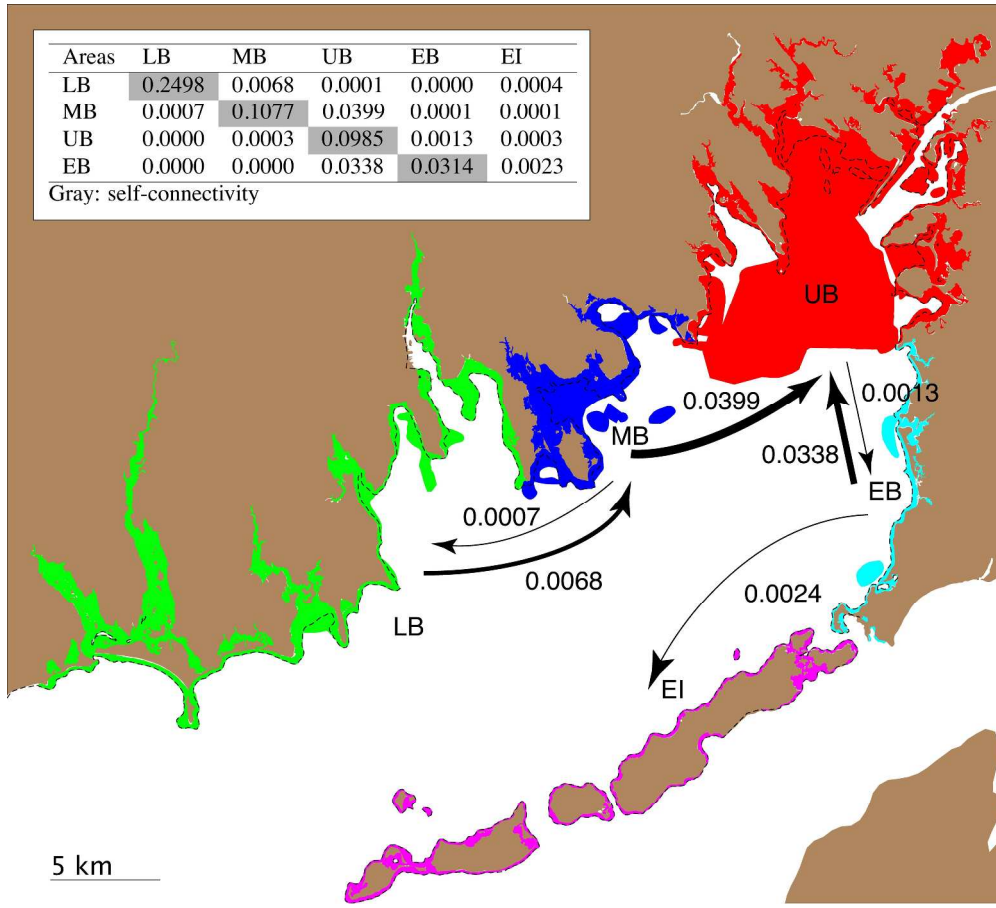

Schematic diagram of connectivity pattern among grouped regions representing the average outcome over the six realistic cases. Numbers indicate the connectivity levels for the corresponding spawning-to-settlement regions. Colored regions represent spawning zones. Dashed lines indicate the extent of the 3.5 m isobath containing the settlement zones.
300x269mm (300 x 300 DPI)

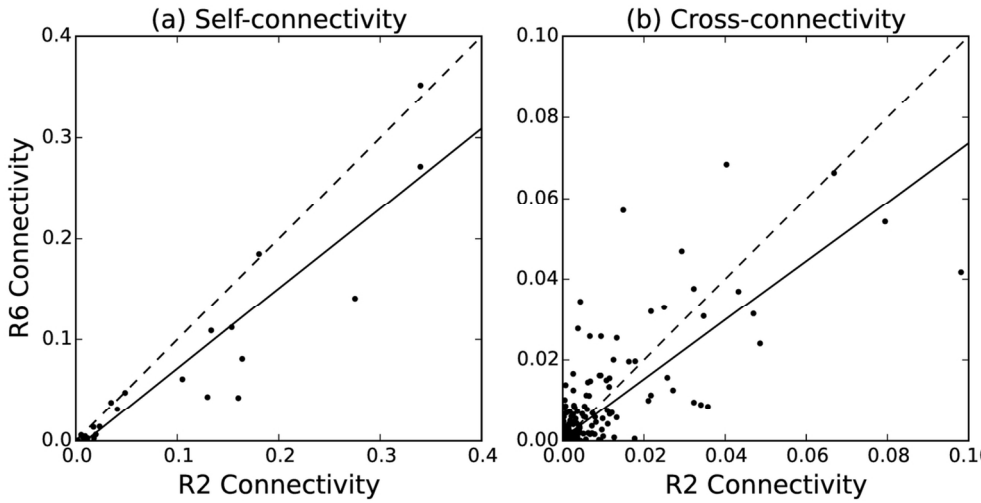

Plots of Case R2 connectivities against Case R6 connectivities, with self- and cross-connectivities plotted in (a) and (b), respectively. Dashed lines represent 1:1 ratios. The least-squares linear fit to the points shown is displayed as a solid line.
113x58mm (300 x 300 DPI)

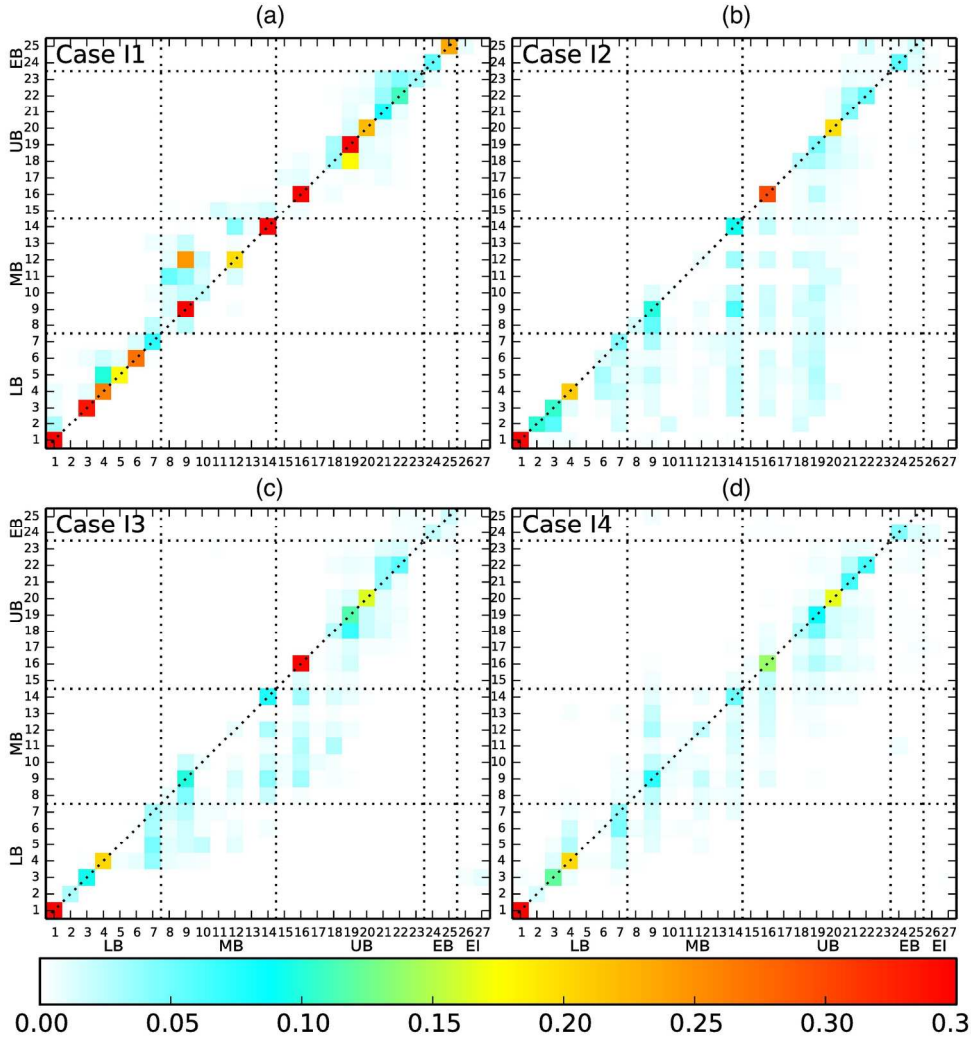

Connectivity matrices for the idealized model runs (I1-I4, Table 1). Elements of each matrix correspond to the settlement success of larval transport from a given spawning zone (the vertical axis) to a given settlement zone (the horizontal axis). Zone numbers are defined in Figs. 3. Dashed horizontal and vertical lines denote larger regions consisting of geographically distinct zones (see text in the Model experiments subsection).

181x190mm (300 x 300 DPI)

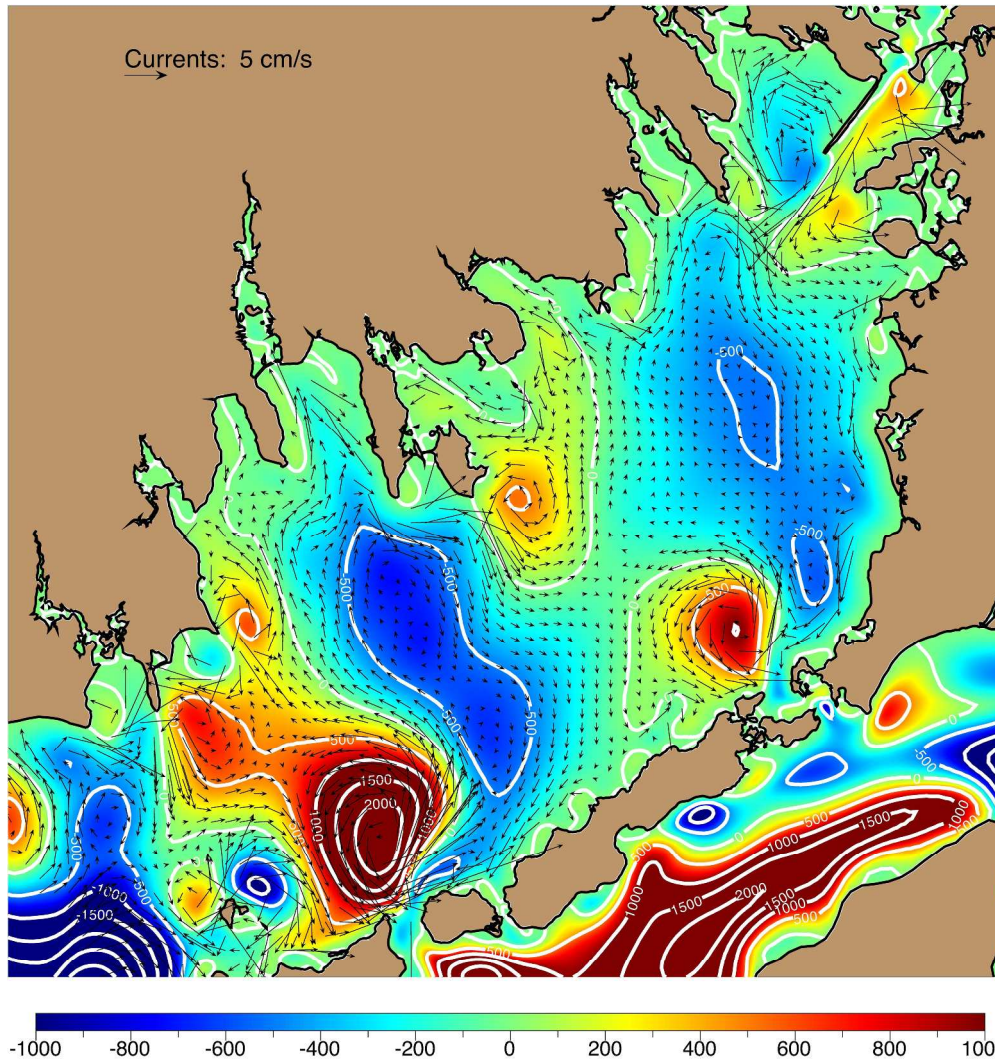

Same as Fig. 4 except showing the model-computed time- and vertically- averaged velocity field (black arrows) of the spawning event forced by a NW-dominant
wind (Case I4). Streamfunctions (in m3/s) computed using the velocity fields of each case are rendered with white contours. The contour interval is 500 m3/s.
318x337mm (300 x 300 DPI)

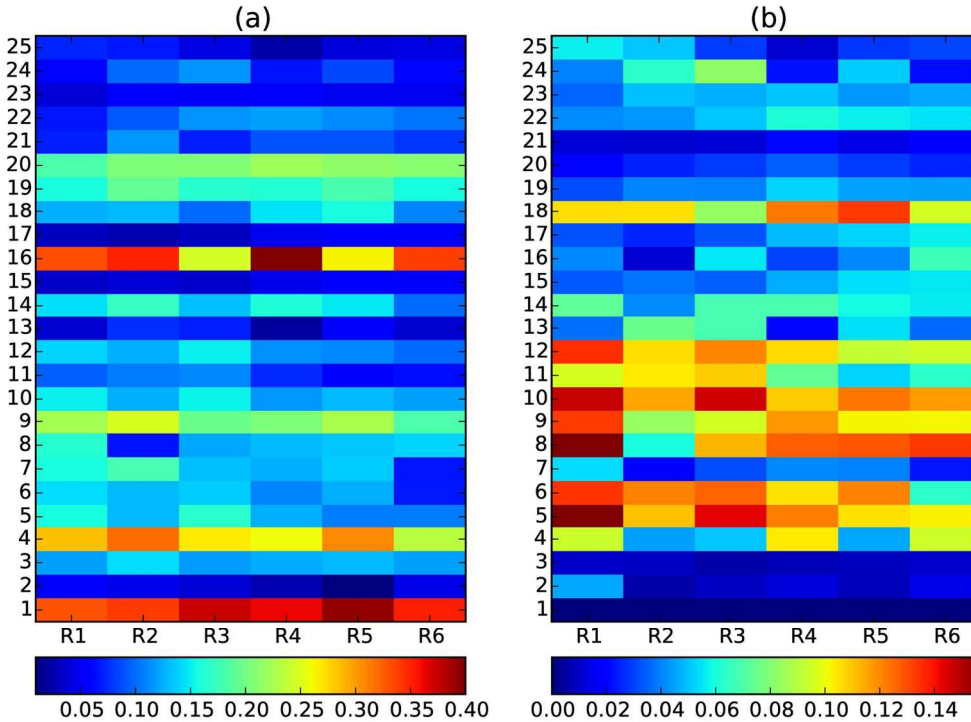

Zone settlement success (Eq. 9) for the six realistic cases from all 25 spawning zones (Fig. 3a); (a) ZSSall, the settlement success to all settlement zones, (b) ZSScc, the settlement success without inclusion of self-connectivity.
153x112mm (300 x 300 DPI)

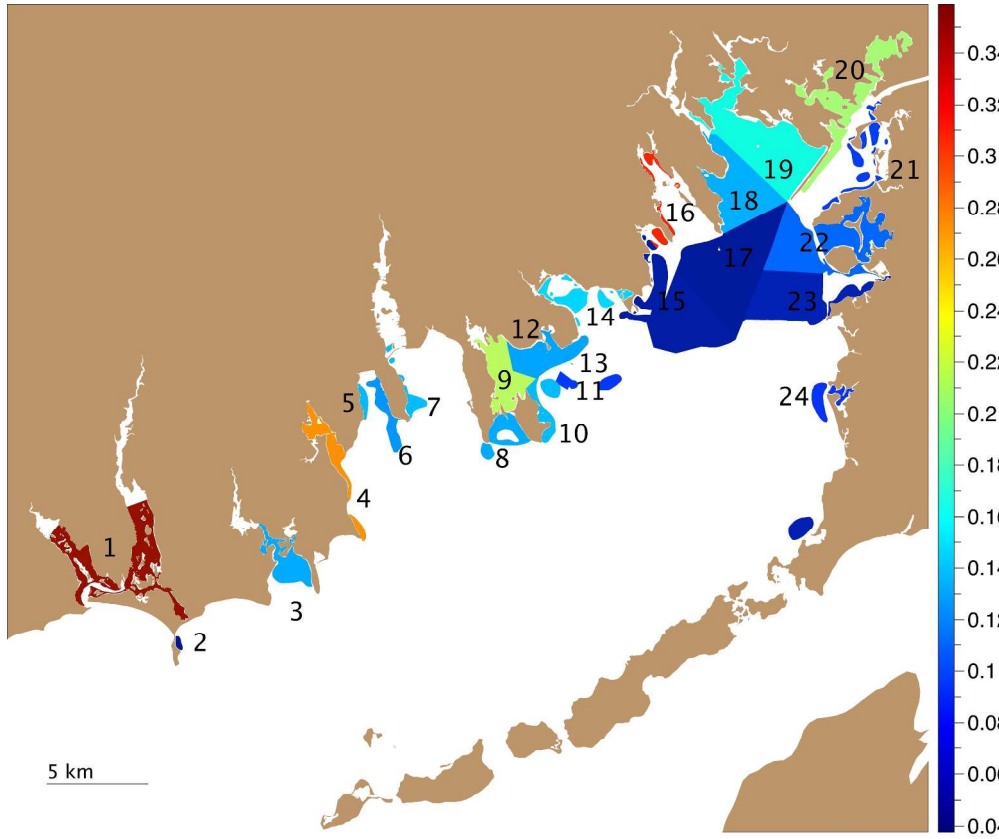

Geographic map of zone settlement success (ZSSall) averaged over over the six realistic cases.
280x234mm (300 x 300 DPI)

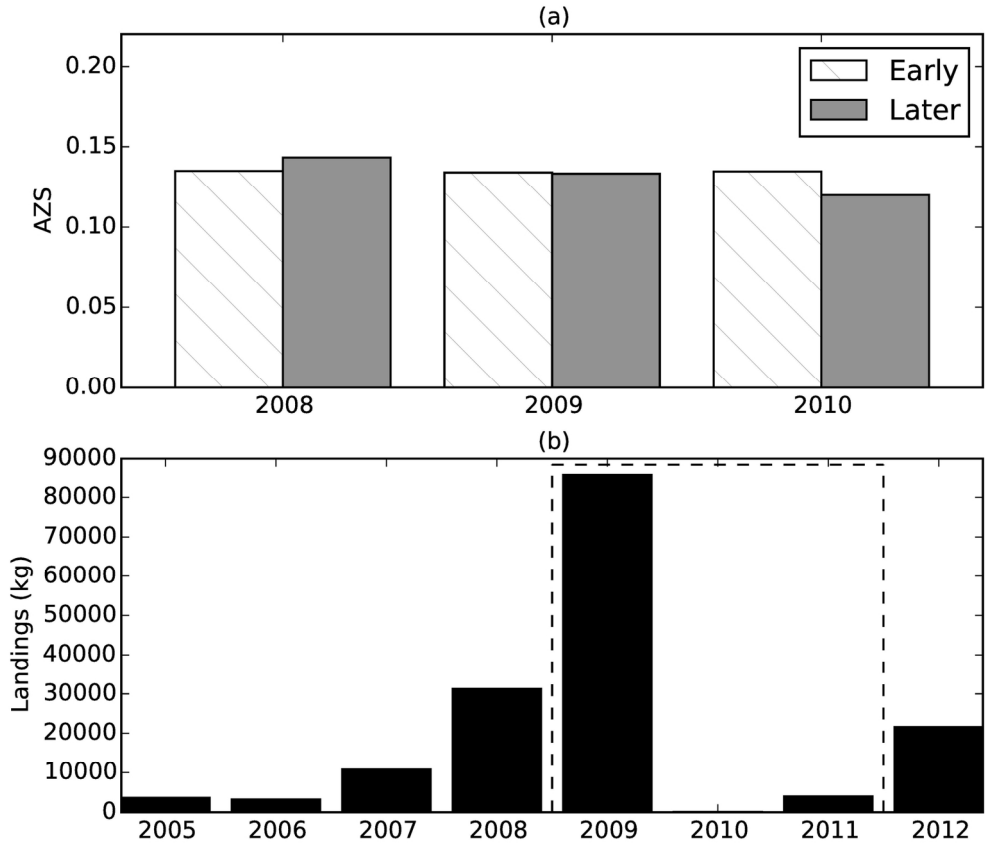

The AZS (arithmetic mean of ZSS over all spawning zones) of the six realistic cases (a) and commercial bay scallop landings in Buzzards Bay (source: Massachusetts Division of Marine Fisheries) (b). The dashed line box encloses the landings of 2009-2011, which would have been the product of spawning over 2008-2010.
157x135mm (300 x 300 DPI)